Journal of Colloid and Interface Science 415 (2014) 70–76

Contents lists available at ScienceDirect

Journal of Colloid and Interface Science

www.elsevier.com/locate/jcis

Photo-cured PMMA/PEI core/shell nanoparticles surface-modified with Gd–DTPA for T1 MR imaging

Montri Ratanajanchai [a,b], Don Haeng Lee [a,c,*], Panya Sunintaboon [b,d], Su-Geun Yang [e,*]

[a] Utah-Inha DDS and Advanced Therapeutics, B-403 Meet-You-All Tower, Songdo Technopark, 7-50, Songdo-dong, Yeonsu-gu, Incheon 406-840, Republic of Korea
[b] Department of Chemistry, Faculty of Science, Mahidol University, Nakhon Pathom 73170, Thailand
[c] Department of Internal Medicine, School of Medicine, Inha University, Incheon 420-751, Republic of Korea
[d] Center of Excellence for Innovation in Chemistry, Faculty of Science, Mahidol University, NakhonPathom 73170, Thailand
[e] Clinical Research Center, School of Medicine, Inha University, 2F A-dong, Jeongseok Bldg., Sinheung-dong 3-ga, Jung-gu, Incheon 400-712, Republic of Korea

ARTICLE INFO

Article history:
Received 28 May 2013
Accepted 28 September 2013
Available online 17 October 2013

Keywords:
Gd–DTPA
Polymethyl methacrylate (PMMA)
Polyethyleneimine (PEI)
Core/shell nanoparticles
MRI
Photo-cured nanoparticles
T1 contrast
Liver cancer
Gd(III)

ABSTRACT

Herein, we introduced amine-functionalized core–shell nanoparticles (Polymethyl methacrylate/Polyethyleneimine; PMMA/PEI) with surface primary amines (3.15×10^5 groups/particle) and uniform size distribution (150–200 nm) that were prepared by one-step photo-induced emulsion polymerization. Further PEI-surface was modified with diethylenetriamine pentaacetic acid (DTPA) and introduced with Gd(III). The modified particles possessing DTPA can entrap a high content of Gd(III) ions of over 5.5×10^4 Gd/particle with stable chelation (no release of free Gd) at least 7 h. The Gd–DTPA-conjugated core–shell nanoparticles (PMMA/PEI–DTPA–Gd NPs) enhanced the MRI intensity more than Primovist (a commercial hepatic contrast agent). Moreover, the PMMA/PEI–DTPA–Gd NPs showed non-cytotoxicity up to 250 μM in normal liver cells. Thus, in vitro data suggested the PMMA/PEI–DTPA–Gd NPs is promising delivery system as a superior MRI contrast agent, especially for hepatic lesion targeted MR imaging.

1. Introduction

In visualization of soft tissue, magnetic resonance imaging (MRI) is considered an efficient technique that provides good three-dimensional images (high spatial resolution < 1 mm) without the use of radioactive compounds or high energy X-rays [1,2]. The contrast of MRI images is directly related to the difference in water proton relaxation rates of various soft tissues [1–3]. However, compounds called 'MRI contrast agents' are required to enhance the image contrast to distinguish lesion areas from normal tissues, especially in cancer diagnosis [3]. Among these, gadolium (Gd) chelates are the most commonly used MRI contrast agents as T1 agents and many have been approved for clinical use [3,4]. Nevertheless, due to their low molecular weight, one major problem with these agents is their short-lived time in blood circulation that limits their MRI efficacy. For example, Gd(III)–diethylenetriamine pentaacetate complex (Gd–DTPA) is rapidly excreted *via* renal filtration and its concentration in blood circulation decreases over 80% within 1 h after intravenous administration [5], which allows less time for MRI observation. One way to overcome this problem is to conjugate these low molecular weight agents with macromolecules such as polysaccharides [6,7], polypeptides [8], synthetic polymers [9,10], synthetic dendrimers [11,12], and synthetic particles [13,14]. Most of them improve the residence time in blood circulation and increase the relaxivity of water protons in the environment.

Moreover, the macromolecular Gd complexes enhance the image contrast in cancer diagnosis because the morphologies of tumor and normal tissues are quite different [3,15]. In general, the large size of macromolecular compounds can influence their biodistribution due to the differences in the vascular systems of tumor tissues compared to normal tissues. In tumors, vascular hyperpermeability allows large particles to diffuse through blood vessels and those particles accumulate in the tissue due to ineffective lymphatic drainage. This phenomenon, called the enhanced permeation and retention (EPR) effect [16,17], leads to greater concentrations of large compounds in tumors than in normal tissues. However, this principle does not explain the size-dependent distribution in some tissues involving the reticuloendothelial system, such as in liver and spleen. In such organs, large particles tend

* Corresponding authors. Address: Division of Gastroenterology & Hepatology, Department of Internal Medicine, Inha University Hospital, Incheon 400-712, Republic of Korea. Fax: +82 32 890 2549 (D.H. Lee). Address: Department of new drug development and NCEED, School of Medicine, Inha University, Incheon 400-712, Republic of Korea. Fax: +82 2 890 1199 (S.G. Yang)
E-mail addresses: ldh@inha.ac.kr (D.H. Lee), Sugeun.Yang@inha.ac.kr (S.-G. Yang).

0021-9797/$ - see front matter © 2013 Elsevier Inc. All rights reserved.
http://dx.doi.org/10.1016/j.jcis.2013.09.049

to localize in normal areas, where the reticuloendothelial network is still intact, more than in tumors [13,18].

In this work, a polymeric nanoparticle was selected as the precursor for preparing the macromolecular contrast agent. We introduced a facile one-step method of photo-induced surfactant-free emulsion polymerization (SFEP) to prepare PMMA-core/PEI-shell nanoparticle (PMMA/PEI NPs, Scheme 1A). This core/shell NPs possessed a high density of surface amine groups (PEI) with homogeneous size and higher stability in aqueous solution. PMMA/PEI NPs were modified with diethylenetriamine pentaacetic acid (DTPA) *via* amide coupling reaction using water-soluble carbodiimide-activating system [19]. And further Gd(III) ions were chelated on the DTPA moieties to get T1 imaging agents (PMMA/PEI–DTPA–Gd NPs, Scheme 1B). In vitro T1 contrast activity of PMMA/PEI–DTPA–Gd NPs and its cytotoxicity in normal liver cells were evaluated in this study.

2. Experimental

2.1. Materials

Methyl methacrylate (MMA), branched polyethyleneimine (PEI; 50 wt% solution in water, Mn = 60 000, Mw = 750,000), camphorquinone (CQ, bornanedione,1,7,7-trimethylbicyclo [2.2.1] heptane-2,3-dione), l-ethyl-3-(3-dimethylaminopropyl) carbodiimide hydrochloride (EDC), N-hydroxysuccinimide (NHS), and gadolinium chloride ($GdCl_3$) were all obtained from Aldrich. MMA was purified by vacuum distillation after removing inhibitor by NaOH extraction. Diethylenetriamine pentaacetic acid (DTPA) was purchased from TCI Company.

2.2. Photo-polymerization of PMMA/PEI core/shell nanoparticles

PMMA/PEI core/shell nanoparticles were synthesized *via* photo-induced SFEP as shown in Scheme 1A. The polymerization was conducted in a 100-mL water-jacketed flask equipped with a nitrogen inlet–outlet, water-circulating thermostat, and magnetic stirrer. First, 5 g of 10 wt% PEI solution was mixed with distilled water. The 600 rpm stirred mixture was purged with nitrogen gas for at least 30 min. Temperature-controlled water (25 °C) was pumped through the jacketed reactor from the thermostat. After that, 2 mL of the purified MMA was added into the reactor, followed by 1 mL of 0.02 M CQ. The total volume of the reaction was 50 mL. All steps were done in a dark room. The mixture under nitrogen was exposed to visible-light from the halogen floodlight (SP. Electric) in a tubular lamp (Sylvania) for 3 h. The distance from the light tube to the center of the reactor was 25 cm. The MMA conversion was determined gravimetrically. Unbound PEI molecules in the synthesized nanoparticles were removed by ultracentrifugation at 25,000 rpm. All supernatants from centrifugation were collected to determine % grafted PEI by TNBS assay.

2.3. Physical characteristics of PMMA/PEI core/shell NPs

Hydrodynamic diameters and surface charges were then measured by using a zetasizer (zetasizer 3000, Malvern Instruments) at 25 °C. pHsof medium were adjusted to be in the range of 3–12. Then, their corresponding ζ-potentials were measured and plotted with varying pH values. Isoelectric point (pI) of NPs was determined as the pH at which the ζ-potential was zero.

Core/shell structure of NPs was observed on a transmission electron microscopy (TEM; Phillip, CM-200, 120 kV). PMMA/PEI NPs were diluted 100-fold with distilled water, 20 μL of the diluted sample was then deposited on copper grids and stained with 2 wt% phosphotungstic acid (PTA; Fluka) [20–22]. Furthermore, the TEM images were also used to calculate the number of particles per volume (Np) as in the following equation [23]:

$$\mathrm{Np} = \frac{\text{Total volume of PMMA}}{\text{Volume of core PMMA per particle}} = \frac{m_p/\rho_p}{\frac{\pi}{6}(D_{cv})} \quad (1)$$

where m_p is the total mass of polymerized monomer (mg/mL^{-1}), ρ_p is the density of PMMA core (1.19 g/cm^3). The volume-average diameter of the core compartment (D_{CV}) was determined from at least 100 particles in TEM images. Next, the percentage of grafted PEI (G_{PEI}), the 1°-amine per particle (NP-NH_2), and 1°-amine concentration were determined by The modified 2,4,6-trinitrobenzene sulfonic acid (TNBS; Aldrich) assay (see the supporting information).

2.4. Conjugation of DTPA onto the PEI shell

The DTPA-functionalized core/shell nanoparticles (PMMA/PEI–DTPA NPs) were prepared by amide coupling reaction between the amine groups of PEI shell and the carboxylic groups of DTPA using EDC/NHS activating system. The pre-optimized molar ratio between DTPA per 1°-amine was 5:1. First, PMMA/PEI was prepared to contain 20 mM of 1°-amine (~3.8×10^{13} particles/mL) and adjusted to pH 6 by 0.1 M HCl. Next, 8 mL of the solution

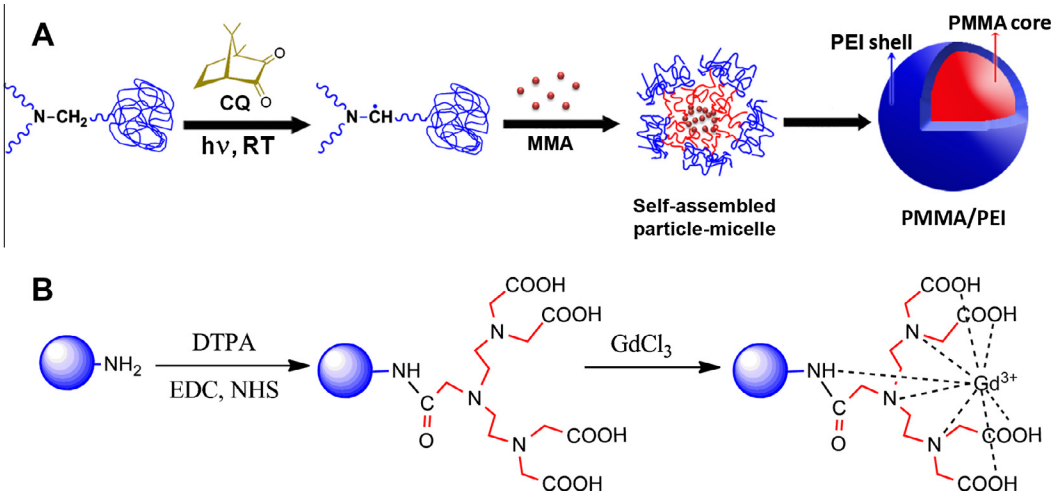

Scheme 1. (A) Formation of PMMA/PEI core/shell nanoparticles *via* the photo-induced SFEP using CQ/PEI initiating system. (B) Conjugation of Gd-DTPA on the PEI-shell surface. The acquired PMMA/PEI–DTPA–Gd NPs were further investigated for the development of hepatic lesion-targeted T1 contrasting agent, and subjected to the serial in vitro studies including T1 contrast phantom study, hepatic cell uptake study and cytotoxicity study.

was mixed with 2 mL of 0.4 M DTPA for 30 min. Afterwards, 2 mL of 0.8 M EDC and 2 mL of 0.4 M NHS were added and stirred for 6 h at room temperature. The product was adjusted to a pH of about 7 and then purified by ultracentrifugation. The amount of covalently bound DTPA on the particle surface was calculated based on a modified toluidine blue O (TBO) assay [24,25] (see the supporting information).

2.5. Chelation of gadolinium (Gd) onto the DTPA units

To introduce Gd (III) ions onto the particles, $GdCl_3$ as a Gd precursor was reacted with nanoparticles that have DTPA as a ligand unit. The complexation was performed in citrate buffer (0.1 M, pH 5.5) since the precipitation of $GdCl_3$ can take place in neutral or basic pH conditions. In detail, PMMA/PEI–DTPA diluted with 10 mM of carboxylate groups ($\sim 4.0 \times 10^{13}$ particles/mL) was slowly dropped into the solution of citrate buffer containing 6 mM $GdCl_3$ by a syringe pump machine (Longerpump, LSP01-1A) at the rate of 20 μL/min. The final molar ratio of carboxylate and $GdCl_3$ was 1:1. The solution was continuously stirred overnight to reach equilibrium complexation. The Gd(III)–DTPA conjugated core–shell nanoparticles (PMMA/PEI–DTPA–Gd) were then purified to remove excess Gd(III) ions by ultracentrifugation. Moreover, the supernatant from each centrifugal cycle was collected to check for complete removal of free Gd by inductively coupled plasma-optical emission spectroscopy (ICP-OES; SPECTRO GENESIS, Spectro Analytical Instruments GmbH). Hydrodynamic diameters, surface charges, and morphology of Gd-binding product were characterized as described in Section 2.3. The final content of Gd was determined by using anICP-OES (see the supporting information).

2.6. In vitro T1 contrast activity of Gd-DTPA conjugated particle

The paramagnetic property of the prepared polymeric Gd chelate was preliminarily investigated in comparison with Gd-(ethoxybenzyl-DTPA) (Primovist; Bayer Schering Pharma AG). First, PMMA/PEI–DTPA–Gd and Primovist with Gd concentrations ranging from 0 to 256 μM in distilled water were added into 24-well plates. PMMA/PEI and PMMA/PEI–DTPA in the same amount as the Gd-DTPA modified nanoparticles were also observed. Next, the plates were placed in a phantom and introduced into a 1.5 T horizontal scanner (Signa Excite; GE Healthcare, Milwaukee, WI) using a Quadknee coil at room temperature. Scan parameters: T_R = 400 ms, T_E = 25, 50, 100, 200 ms.

2.7. In vitro cytotoxicity in normal liver cells

Chang's liver cell line was maintained in minimum essential media with L-glutamine, ribonucleosides, and deoxyribonucelosides (MEM Alpha; Gibco) containing 10% fetal bovine serum, and 1% streptomycin–ampicillin under 5% CO_2 at 37 °C. To evaluate in vitro cytotoxicity, the cells were seeded at a density of 8×10^3 cells/well (100 μL/well) on 96-well plates. After 24-h incubation, the cells were treated with 100 μL of various concentrations (2-fold dilution) of samples in media and then incubated for 2 days. Thereafter, the treated media were removed and cells were washed with Dulbecco's phosphate-buffered saline (DPBS; WELGENE). Then the solution was replaced with 100 μL of 10-fold diluted solution of Ez-Cytox reagent (DAEIL lab service) in media. After 90-min incubation, the absorbance of the plates was measured at 490 nm on the micro-plate reader (Synergy Mx, Biotek). The % cell availability of each condition was reported for 4 independent experiments compared with control media.

2.8. Cell uptake study

To evaluate cellular internalization in vitro by confocal laser scanning microscopy (CLSM), PMMA/PEI–DTPA–Gd was labeled with *N*-succinimidyl carboxyfluorescein (NHS-fluorescein, Thermo Scientific) (see the supporting information). Chang's liver cells were seeded on 22×22 mm^2 coverslips placed in 6-well plates at density of 1×10^5 cells/well. After incubation under 5% CO_2 at 37 °C for 1 day, the cells were treated by the fluorescently labeled PMMA/PEI–DTPA–Gd containing 250 μM Gd in media. After 1 h incubation at 37 °C in 5% CO_2 atmosphere, the cells were washed twice with PBS and fixed with 4 wt% paraformaldehyde (Merck) in PBS for 30 min and then washed with 1 wt% Tween20 in PBS. Finally, the coverslips were mounted on glass slides using mounting medium with 1.5 μg/mL of DAPI (Vectashield H-1500; Vector Laboratories). The slides were observed by confocal microscopy (Leica Microsystems) using a 40× oil immersion objective.

3. Results and discussion

3.1. Properties of PMMA/PEI nanoparticles

The amine-functionalized nanoparticles were prepared *via* surfactant-free emulsion polymerization (SFEP) induced by the CQ/3°-amine photo-initiating system. The mechanistic scheme of the particle formation is shown in Scheme 1A and is quite similar to the core–shell particle formation by the thermally-induced SFEP system published in recent decades [23,26]. In brief, CQ photo-initiator was excited by visible-light photons and then reacted with 3°-amine of PEI molecules to generate initiating radicals. The active radicals on PEI chains initiated polymerization of MMA monomers that resulted in the PMMA/PEI graft-copolymer chains. In aqueous solution, the copolymers oriented themselves thermodynamically to form micelle-like micro-domains where PEI segments face the water and PMMA hydrophobic segments face the inside of the micelles. Thereafter, the propagating radicals of core PMMA chains propagated other MMA monomers in the system that provided core–shell nanoparticles as the final product. The MMA monomer conversion was about 83% (Table 1).

From TEM images (Fig. 1A), the PEI-immobilized nanoparticles exhibited a core–shell structure with a uniform size of ~150 nm, which was consistent with the hydrodynamic diameter measured by Zetasizer (Table 1). Then, we assayed the particle stability and found that the PMMA/PEI core/shell NPs showed great stability (ζ-potential higher than 40 mV) in neutral and acidic conditions (Fig. 2), which will allow a wide range of pHs in many applications.

Next, we developed a TNBS assay to measure the percentage of grafted PEI (G_{PEI}) in the polymerization by determining free PEI in the supernatants. The G_{PEI} was ~70%, indicating that more than half of the total PEI was permanently bound onto PMMA/PEI

Table 1
Characteristics of PMMA/PEI core–shell nanoparticles prepared *via* photo-induced SFEP[a] ($n \geqslant 3$; mean ± SEM).

Product characteristics	Value
% MMA, involved in photo polymerization	82.9 ± 2.56
Volume-average diameter of core (PMMA), D_{cv} (nm)[b]	86.6 ± 9.39
Percentage of grafted PEI, G_{PEI} (%)	69.2 ± 5.65
1°-amine groups per particle, NP-NH_2 (10^5)	3.15 ± 0.28
Number-averaged diameter, D_n (nm)[c]	189.1 ± 18.8
Particle size distribution, D_v/D_n[c]	1.381 ± 0.117
ζ-potential (mV)[d]	43.0 ± 0.873

[a] Synthesis condition: 1 wt% PEI, 4 wt% MMA, 0.4 mM CQ, 300 W, 3 h reaction.
[b] The PMMA core diameter was averaged from TEM images.
[c] Values were determined in wet state by Zetasizer analyzer.
[d] To assess shelf-life of the product, the measurement was performed without pH adjustment.

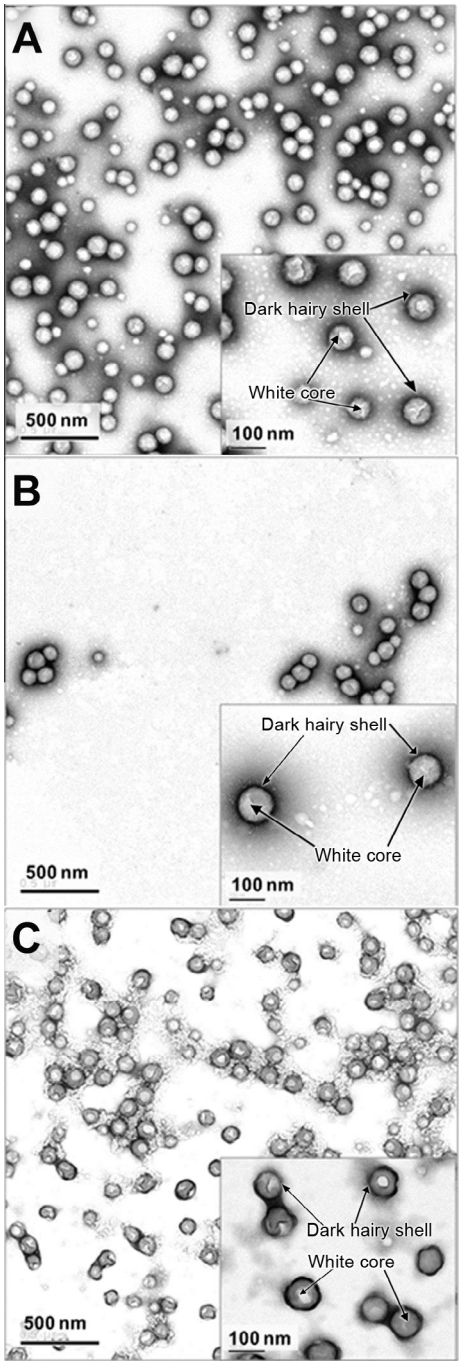

Fig. 1. The particle morphology observed by TEM of (A) PMMA/PEIcore/shell NPs, (B) DTPA-surface modified PMMA/PEI NPs, and (C) PMMA/PEI–DTPA–Gd NPs. The high magnification is shown in the inset images. Decreased mean particles size was observed after the Gd-chelation (Tables 1 and 2), and it seemed to be from condensation of shell-surface.

(Table 1). The TNBS assay also provided the 1°-amine per particle (NP-NH_2) and 1°-amine concentration. We found that more than 300,000 groups of 1°-amine were available on the surface and useful for further modification. The molar concentration of 1°-amine was 40 mM for PMMA/PEI with 7.7×10^{13} particles/mL.

3.2. PEI-surface modification with DTPA through amide coupling reaction

As described, the PEI-immobilized particles have surface amine groups that can be modified by various molecules. Herein, we focused on modifying the particles to form the Gd-based MRI contrast agent. There are many approaches for conjugating MRI contrast agents onto amine-functionalized polymers [6,11,12,18,27]. Because the obtained particles were dispersed in aqueous medium, modification methods using organic solvents were difficult and led to destabilization of the particles. To avoid this problem, an amide coupling reaction using water-soluble carbodiimide activating system was selected since this method used mild conditions without organic solvent, inert gas, and/or high temperature [19,28].

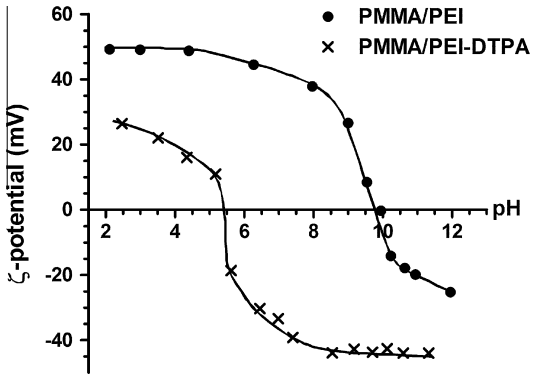

Fig. 2. pH-dependent ζ-potentials of PMMA/PEI core–shell nanoparticles before and after conjugation of DTPA (− charge) with surface-PEI (+ charge).

We introduced DTPA, which is a widely used ligand for Gd and possesses 5 carboxylate groups for coupling reaction. Nevertheless, optimal conditions for the modification must be found in order to keep at least 3 COOH units that are required for chelating Gd similar to commercial Gd-(DTPA bisamides) [29] and still maintain the particle stability after modification. Accordingly, the molar ratio of DTPA:EDC:NHS was 1:2:1 to ensure that the conversion was limited to one or two carboxylate group(s). Furthermore, the molar ratio of DTPA to 1°-amine of PMMA/PEI was 5:1 because our preliminary study (results not included) suggested that this molar ratio provided products with good stability (ζ-potential lower than −30 mV) and uniform size distribution after the modification.

The amide formation between carboxylate of DTPA and amine groups of PMMA/PEI was confirmed by many techniques, for example, ζ-potential and TEM. The ζ-potential of the particles modified with DTPA (Fig. 2) was dramatically reduced compared to that of unmodified PMMA/PEI. The pI of the DTPA-modified particles was shifted from 10 to 5.5, indicating that the amine groups on the PMMA/PEI's surface were modified with carboxylate groups of DTPA [30]. The covalent functionalization of DTPA onto PMMA/PEI was further supported by TEM images (Fig. 1B) using UAc as a staining agent. Although the PMMA/PEI was modified with DTPA, the morphology still provided a core–shell structure. The shell stained by cationic UAc implied availability of DTPA on the particles' surface [31]. The hydrodynamic size and size distribution (Table S1) of the PMMA/PEI–DTPA did not change much from those of the parent particles.

Next, we applied TBO onto the DTPA-functionalized particles to estimate the amount of carboxylate groups on their surface. As described previously, TBO is commonly used as a cationic dye; it adsorbs onto anionic surfaces and exhibits a color change from blue to red-violet called 'metachromasy' [24,30]. This also occurred when TBO was added into the purified PMMA/PEI–DTPA (Fig. 3), which supported the functionalization.

Herein, we designed the TBO assay to determine maximum TBO adsorption onto PMMA/PEI–DTPA's surface. The equilibrium TBO adsorption onto the modified particles (Q_e; mol/particles) at each point was calculated by the following equation:

$$Q_e = \frac{(C_0 - C_e)V}{\text{total particles}} = 2.09 \times 10^{-15}(C_0 - C_e) \quad (2)$$

where the C_0 and C_e is the total and equilibrium molar concentrations of TBO in the solution at a certain point, V is the total volume (0.05 L), and the total number of DTPA-functionalized particles in the experiment was 2.4×10^{13} particles.

Next, the adsorption data (Table S2) were well fitted by Langmuir's adsorption model. So, we applied this model to find the maximum adsorption of TBO onto the particles (Q_m, mol/particle) according to the following equation:

$$\frac{C_e}{Q_e} = \frac{C_e}{Q_m} + \frac{K_d}{Q_m} \tag{3}$$

where K_d is the dissociation constant. From the plot of C_e/Q_e versus C_e, the fitting curve's slope and y-intercept were defined as $1/Q_m$ and K_d/Q_m, respectively (Fig. S1).

The observed Qm was 25.14×10^{-20} mol/particle indicating that there were 1.51×10^5 carboxylate groups/particle. Thus, the molar concentration of COOH was around 10.1 mM for the PMMA/PEI–DTPA sample with 4×10^{13} particles/mL.

3.3. Chelation of DTPA-functionalized nanoparticles to Gd(III)

Because $GdCl_3$ is less water-soluble at, near or above neutral pH [32,33]. But PMMA/PEI–DTPA has low stability in acidic conditions, the stability of both components during complexation is a concern. Our first attempt of slowly adding $GdCl_3$ solution into the DTPA-modified particle at neutral pH provided poor product with large aggregation. We therefore altered the method by slowly adding the DTPA-modified particles into the $GdCl_3$ solution (controlled pH at 5.5 by citrate buffer). The chelated product after purification showed good texture without too much aggregation of particles and a core–shell structure (Table 2 and Fig. 1C). The slight decrease in size was caused by shrinkage of the shell segment under chelation.

Next, we determined Gd content in the Gd–DTPA conjugated nanoparticles (PMMA/PEI–DTPA–Gd) by ICP-OES using $GdCl_3$ for calibration curve (Fig. S2A). The product was purified by centrifugation to remove all unbound Gd (complete removal confirmed by remaining Gd in each supernatant cycle as shown in Fig. S2B). At a concentration of 2.4×10^{13} particles/mL, the average concentration of Gd was 2.21 mM, indicating that there were more than 55,000 Gd(III) ions/particle (Table 2). The Gd content of our particles was much higher than that in dendrimer-based Gd chelates [11,12,27] and slightly higher than polymeric Gd particles having size around 100–200 nm [34,35] but much lower than Gd-conjugated dendrimer nanocluster [34]. However, we believe that the core–shell structure of PMMA/PEI–DTPA–Gd NPs has the potential to be used as a multi-functional MRI contrast agent.

3.4. Paramagnetic properties of PMMA/PEI–DTPA–Gd NPs

The paramagnetic properties of PMMA/PEI–DTPA–Gd NPs were next evaluated in comparison with Primovist and the particles without Gd. In the present work, we focused on liver tissue because it is a vital organ and can entrap large-sized compounds in its reticuloendothelial system [36]. Thus, Primovist, an FDA-approved and liver-specific MRI contrast agent [37,38], was selected as a model for small Gd complexes. The result (Fig. 4) showed that the Gd-DTPA modified particles enhanced the intensity in the MRI image to a higher level than Primovist, and the optimal concentration for MRI application is at least 32 μM (see exponential curve in Fig. 4B) for the scan parameters: 1.5 T, 25 °C, T_R = 400 ms, T_E = 25 ms. Neither precursor particle (PMMA/PEI–DTPA or PMMA/PEI) strongly affected the MRI intensity and both exhibited concentration-independent image intensity. The longitudinal relaxivities (r_1) of both PMMA/PEI–DTPA–Gd and Primovist were also determined by plotting relaxation rates against Gd concentration (Fig. 4C) and the values were calculated using the following equation:

$$(1/T_1)_x = (1/T_1)_0 + r_1 \cdot [\mathrm{Gd}]_x \tag{4}$$

where $[Gd]_x$ is the concentration of Gd (μM) in the solution, $(1/T_1)_x$ and $(1/T_1)_0$ are the relaxation rates at $[Gd] = x$ and without Gd, respectively.

The relaxivity of the Gd–DTPA modified particles was 1.75 times that of the small contrast agent (34.28 and 19.59 $mM^{-1}\,S^{-1}$ for PMMA/PEI–DTPA–Gd and Primovist, respectively). In general, the conjugation of small Gd complexes to macromolecules can enhance MRI intensity by increasing the water proton relaxivity

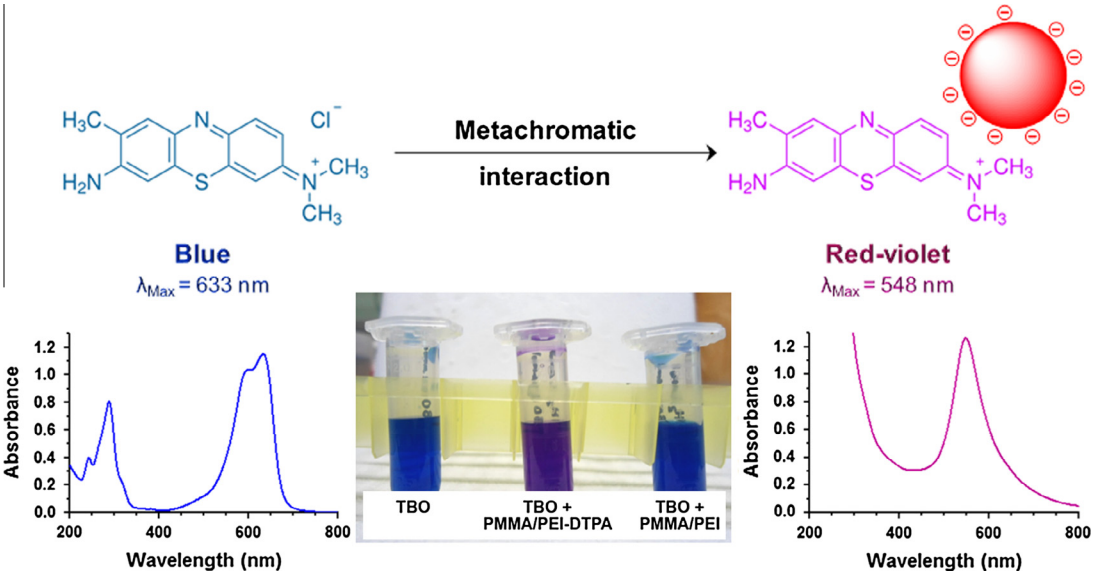

Fig. 3. DTPA-surface modification of PMMA/PEI core/shell nanoparticles; metachromasy of TBO under staining to anionic PMMA/PEI–DTPA particles. Color changes with hypsochromic shift of TBO from original blue (λ_{max} = 633 nm) to red-violet (λ_{max} = 548 nm) informed an interaction between TBO and PMMA/PEI–DTPA's surface (− charge), whereas there is no change in the presence of PMMA/PEI (+ charge). (For interpretation of the references to color in this figure legend, the reader is referred to the web version of this article.)

Table 2
Properties of PMMA/PEI–DTPA–Gd core/shell nanoparticles ($n \geqslant 3$; mean ± SEM).

Product characteristics	Value
Number-averaged diameter, D_n (nm)[a]	146.7 ± 8.25
Particle size distribution, D_v/D_n[a]	1.482 ± 0.141
ζ-potential (mV)[b]	−3.17 ± 1.17
Gd/particle (10^4)[c]	5.53 ± 0.202
Gd concentration (mM) [c]	2.21 ± 0.081

[a] Values were determined in wet state by Zetasizer analyzer.
[b] The Gd-binding particle was adjusted to pH 7.4 before measurement.
[c] Data were obtained from ICP-OES.

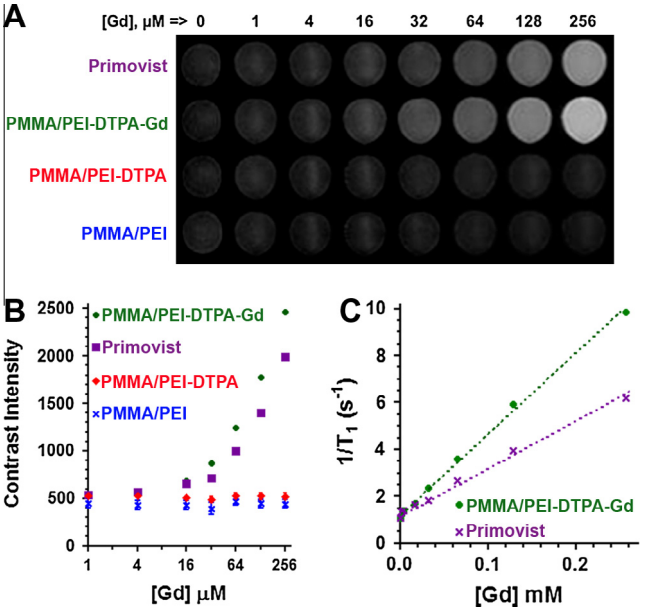

Fig. 4. (A) Concentration dependent T1 contrast in MR phantoms study (Primovist, PMMA/PEI–DTPA–Gd NPs, PMMA/PEI–DTPA NPs, and PMMA/PEI NPs). For PMMA/PEI–DTPA NPs and PMMA/PEI NPs, the concentrations in units of particles per mL were prepared to be equal to that of the Gd-binding particle. (B) Graph plotted by image intensities (determined using Onis viewer software) against Gd concentrations at T_E = 25 ms. (C) Relaxation rates vs. Gd concentrations of Primovist and PMMA/PEI–DTPA–Gd NPs. The dotted lines are the fitted curve (n = 5; mean ± SEM).

[7,13,18,39]. This occurs by 2 main mechanisms: inducing an increase of local water density leading to a higher water exchange rate and/or amplifying Gd density due to greater loading capacity of Gd per molecule [29,40]. Since PMMA/PEI–DTPA did not show significant enhancement of the image intensity itself, the larger Gd content per particle seemed to be the major reason for the higher relaxivity of the Gd–DTPA modified particles.

3.5. Free Gd release of PMMA/PEI–DTPA–Gd NPs

Many literatures reported that Gd(III) ions in the complexes were able to be released from the complexes themselves, leading to the toxicity to the cells [41,42]. Moreover, free Gd also has a potential to accumulate in the membranes, enzymatic structures, and bones, resulting in undetermined long-term consequence [43]. Thus, the release of free Gd from the complexes is clinical importance. In vitro-release profiles of free Gd in distilled water were shown in Fig. S3 (see the experimental procedure in the supporting information). The amount of free Gd released was presented as percentage release in a period of 24 h In the case of PMMA/PEI–DTPA–Gd NPs, it was found that there are scarcely Gd release from the nanoparticles within 7 h. This was caused by the strong conjugation between carboxylate groups on DTPA moieties and Gd(III) ions. However, after 1 day incubation, the free Gd release was significantly increased up to 10%. Although the Gd(III) ions were strongly bound with DTPA moieties, the chelation of these ions also partially occurred by the amine groups along PEI chains. Theses Gd chelated by PEI had low affinity and, therefore, led to dissociation of the Gd(III) ions. According to this result, it is necessary to observe side effect of the free Gd leaked from the particles by investigating cytotoxicity of the materials at least 24 h.

3.6. Cytotoxicity of PMMA/PEI–DTPA–Gd NPs in liver cell lines

As described above, we used the Gd–DTPA modified particles as a contrast media for liver cancers. In general cases, Gd chelates with larger size and/or hydrophobic component tend to be entrapped and located in the liver tissue, which is the main reticuloendothelial organ [36]. Therefore, the PMMA/PEI–DTPA–Gd NPs showing sub-micron size had a high probability of locating in this organ. On the other hand, it had less opportunity to locate in the cancer area, which has many blood vessels that are hyperpermeable. We hypothesized that the contrast enhancement by PMMA/PEI–DTPA–Gd in the liver cancer diagnosis resulted from an accumulation of this polymeric Gd chelate in normal liver tissue around the lesion area, which had lesser bioavailability. Accordingly, Chang's liver cell line, an appropriate cell model for normal liver, was used to evaluate the cytotoxic effect of PMMA/PEI–DTPA–Gd NPs.

Fig. 5 shows the cell viability of Chang's liver cells after treatment with our materials for 2 days. PMMA/PEI was quite toxic with a median lethal concentration (LC_{50}) of ~20 μM. In biomedical applications, the limitations of PEI are due to high cytotoxicity related to its cationic nature [44,45]. However, neither modified particle (PMMA/PEI–DTPA or PMMA/PEI–DTPA–Gd) showed a cytotoxic effect, because of the functionalized DTPA enveloping the particles' surface as described previously. The PEI-mediated cytotoxicity was therefore concealed in our case. Similar to Primovist, the Gd–DTPA conjugated nanoparticles were non-toxic above the observed concentrations and the maximum non-toxic dose was over 250 μM. The applicable dose seemed sufficient for further in vivo application, in which Gd contrast agents are usually injected at a final concentration of about 30–50 μM (or μmol/kg) [7,8,13,18,27].

3.7. Cellular internalization of the PMMA/PEI–DTPA–Gd NPs

The cellular localization of PMMA/PEI–DTPA–Gd NPs was investigated in Chang's liver cells. The maximum non-toxic dose of the material was applied to observe the cellular response (Fig. 6). At

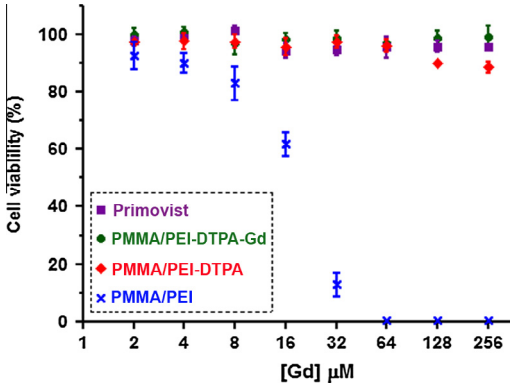

Fig. 5. Dose-dependent cytotoxicity of Primovist, PMMA/PEI–DTPA–Gd NPs, PMMA/PEI–DTPA NPs, and PMMA/PEI NPs in Chang's liver cells (48 h treatment). (n = 4; mean ± SEM). Drastic reduced cellular toxicity was observed after PEI-shell modification with DTPA.

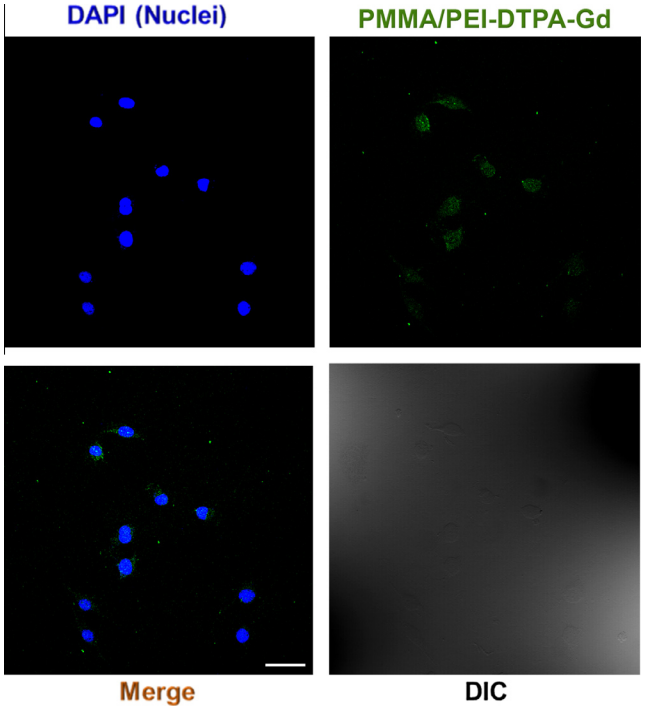

Fig. 6. Intracellular uptake of PMMA/PEI–DTPA–Gd (250 μM, 2 h treatment) on Chang's liver cells. The fluorescent-labeled particles were taken up by the cells (ensured by locating of nuclei labeled with DAPI). Boundary of the cells is shown by differential image contrast (DIC). The scale bar at the right corner of the merge image indicates 100 μm.

high Gd concentration, the polymeric Gd chelate was internalized into the cells and distributed evenly throughout the cytoplasm. Although our macromolecular contrast agent showed negative net charge and was covered by carboxylate groups of the DTPA units, it possessed PEI, which is a well-known cationic polymer that induces gene delivery across the cell membrane [45,46]. Thus, the PMMA/PEI–DTPA–Gd NPs can be taken up by the cells, allowing for intracellular imaging [47,48]. Nevertheless, the cellular internalization of the polymeric contrast agents needs to be optimized since the prolonged accumulation time of polymeric materials also has the potential to lead to greater cytotoxicity.

4. Conclusions

The PMMA/PEI–DTPA–Gd core/shell nanoparticles were synthesized *via* the photo-induced SFEP, a facile one-step preparation, is a promising particle that has reactive amines on its surface; these are essential for chemical modification with various functional-groups including drugs, targeting moieties and peptides. In this study we functionalized these nanoparticles to have Gd–DTPA units without a use of vigorous reactions or organic solvents. PEI along the particles' surface wasconjugated with DTPA units *via* the EDC/NHS activated amide formation and then Gd(III) was introduced into the chelating moiety. And also we observed the enhancement of water proton relaxivity, the reduced cytotoxicity and the high potential for MRI contrast agent. Furthermore, the core–shell structure of this material provides an opportunity to design for hepatic MR contrast agents with multi-functional properties.

Acknowledgments

This work was supported by grants of Medical Scholars Program (MSP), Mahidol University, Thailand and a grant of the Support Project for inducing Foreign Universities or Research Institutions, Ministry of Knowledge Economy and Incheon Free Trade Zone, Republic of Korea.

Appendix A. Supplementary material

Supplementary data associated with this article can be found, in the online version, at http://dx.doi.org/10.1016/j.jcis.2013.09.049.

References

[1] F.A. Jaffer, R. Weissleder, Circ. Res. 94 (2004) 433.
[2] R.B. Lauffer, Chem. Rev. 87 (1987) 901.
[3] C. Khemtong, C.W. Kessinger, J. Gao, Chem. Commun. 24 (2009) 3477.
[4] K.N. Raymond, V.C. Pierre, Bioconjugate Chem. 16 (2004) 3.
[5] H. Weinmann, R. Brasch, W. Press, G. Wesbey, Am. J. Roentgenol. 142 (1984) 619.
[6] V. Darras, M. Nelea, F.M. Winnik, M.D. Buschmann, Carbohydr. Polym. 80 (2010) 1137.
[7] H. Yim, S.-G. Yang, Y.S. Jeon, I.S. Park, M. Kim, D.H. Lee, Y.H. Bae, K. Na, Biomaterials 32 (2011) 5187.
[8] G. Zhang, R. Zhang, M.P. Melancon, K. Wong, J. You, Q. Huang, J. Bankson, D. Liang, C. Li, Biomaterials 33 (2012) 5376.
[9] R.L. Lucas, M. Benjamin, T.M. Reineke, Bioconjugate Chem. 19 (2007) 24.
[10] M.G. Duarte, M.H. Gil, J.A. Peters, J.M. Colet, L.V. Elst, R.N. Muller, C.F.G.C. Geraldes, Bioconjugate Chem. 12 (2001) 170.
[11] R. Xu, Y. Wang, X. Wang, E.-K. Jeong, D.L. Parker, Z.-R. Lu, Exp. Biol. Med. 232 (2007) 1081.
[12] Z. Jászberényi, L. Moriggi, P. Schmidt, C. Weidensteiner, R. Kneuer, A. Merbach, L. Helm, É. Tóth, J. Biol. Inorg. Chem. 12 (2007) 406.
[13] Z. Chen, D. Yu, C. Liu, X. Yang, N. Zhang, C. Ma, J. Song, Z. Lu, J. Drug Target. 19 (2011) 657.
[14] T. Ren, Q. Liu, H. Lu, H. Liu, X. Zhang, J. Du, J. Mater. Chem. 22 (2012) 12329.
[15] H. Maeda, L.W. Seymour, Y. Miyamoto, Bioconjugate Chem. 3 (1992) 351.
[16] Y.H. Bae, K. Park, J. Controlled Release 153 (2011) 198.
[17] Y. Matsumura, H. Maeda, Cancer Res. 46 (1986) 6387.
[18] Y. Liu, Z. Chen, C. Liu, D. Yu, Z. Lu, N. Zhang, Biomaterials 32 (2011) 5167.
[19] N. Nakajima, Y. Ikada, Bioconjugate Chem. 6 (1995) 123.
[20] C.J. Ferguson, G.T. Russell, R.G. Gilbert, Polymer 43 (2002) 6371.
[21] N. Willet, J.-F. Gohy, L. Auvray, S. Varshney, R. Jerome, B. Leyh, Langmuir 24 (2008) 3009.
[22] X. Li, J. Zuo, Y. Guo, X. Yuan, Macromolecules 37 (2004) 10042.
[23] K.M. Ho, W.Y. Li, C.H. Lee, C.H. Yam, R.G. Gilbert, P. Li, Polymer 51 (2010) 3512.
[24] S.-K. Kam, J. Gregory, Colloids Surf. A 159 (1999) 165.
[25] K.M. Gattás-Asfura, D.M. Naistat, R.M. Leblanc, Colloids Surf., A 282–283 (2006) 471.
[26] P. Li, J. Zhu, P. Sunintaboon, F.W. Harris, Langmuir 18 (2002) 8641.
[27] K. Luo, G. Liu, W. She, Q. Wang, G. Wang, B. He, H. Ai, Q. Gong, B. Song, Z. Gu, Biomaterials 32 (2011) 7951.
[28] L.H.H. Olde Damink, P.J. Dijkstra, M.J.A. van Luyn, P.B. van Wachem, P. Nieuwenhuis, J. Feijen, Biomaterials 17 (1996) 765.
[29] P. Caravan, J.J. Ellison, T.J. McMurry, R.B. Lauffer, Chem. Rev. 99 (1999) 2293.
[30] X.-J. Song, J. Hu, C.-C. Wang, Colloids Surf., A 380 (2011) 250.
[31] V. Freger, Langmuir 19 (2003) 4791.
[32] J.L. Barnhart, N. Kuhnert, D.A. Bakan, R.N. Berk, Magn. Reson. Imaging 5 (1987) 221.
[33] A.J. Spencer, S.A. Wilson, J. Batchelor, A. Reid, J. Pees, E. Harpur, Toxicol. Pathol. 25 (1997) 245.
[34] Z. Cheng, A. Tsourkas, Langmuir 24 (2008) 8169.
[35] S. Flacke, S. Fischer, M.J. Scott, R.J. Fuhrhop, J.S. Allen, M. McLean, P. Winter, G.A. Sicard, P.J. Gaffney, S.A. Wickline, G.M. Lanza, Circulation 104 (2001) 1280.
[36] H. Kobayashi, M.W. Brechbiel, Adv. Drug Deliv. Rev. 57 (2005) 2271.
[37] A. Ba-Ssalamah, M. Uffmann, S. Saini, N. Bastati, C. Herold, W. Schima, Eur. Radiol. 19 (2009) 342.
[38] C.J. Zech, K.A. Herrmann, M.F. Reiser, S.O. Schoenberg, Magn. Reson. Med. Sci. 6 (2007) 43.
[39] V.C. Pierre, M. Botta, K.N. Raymond, J. Am. Chem. Soc. 127 (2004) 504.
[40] M. Querol, A. Bogdanov, J. Magn. Reson. Imaging 24 (2006) 971.
[41] J. Künnemeyer, L. Terborg, S. Nowak, A. Scheffer, L. Telgmann, F. Tokmak, A. Günsel, G. Wiesmüller, S. Reichelt, U. Karst, Anal. Chem. 80 (2008) 8163.
[42] W.P. Cacheris, S.C. Quay, S.M. Rocklage, Magn. Reson. Imaging 8 (1990) 467.
[43] W.A. Gibby, K.A. Gibby, W.A. Gibby, Invest. Radiol. 39 (2004) 138.
[44] D. Fischer, Y. Li, B. Ahlemeyer, J. Krieglstein, T. Kissel, Biomaterials 24 (2003) 1121.
[45] D.W. Pack, A.S. Hoffman, S. Pun, P.S. Stayton, Nat. Rev. Drug Discov. 4 (2005) 581.
[46] J. Futami, M. Kitazoe, T. Maeda, E. Nukui, M. Sakaguchi, J. Kosaka, M. Miyazaki, M. Kosaka, H. Tada, M. Seno, J. Sasaki, N.-H. Huh, M. Namba, H. Yamada, J. Biosci. Bioeng. 99 (2005) 95.
[47] N. Nitin, L.E.W. LaConte, O. Zurkiya, X. Hu, G. Bao, J. Biol. Inorg. Chem. 9 (2004) 706.
[48] M. Mascalchi, X.-N. Jin, C. Agen, P. Petruzzi, D. Nardini, C. Tessa, D. Caramella, C. Bartolozzi, Magn. Reson. Imaging 15 (1997) 469.